Astronomy & Astrophysics

LETTER TO THE EDITOR

Extragalactic archaeology with the C, N, and O chemical abundances

Fiorenzo Vincenzo and Chiaki Kobayashi

Centre for Astrophysics Research, University of Hertfordshire, College Lane, Hatfield AL10 9AB, UK
e-mail: f.vincenzo@herts.ac.uk, c.kobayashi@herts.ac.uk

ABSTRACT

We predict how the C, N, and O abundances within the interstellar medium of galaxies evolve as functions of the galaxy star formation history (SFH). We adopt a hydrodynamical cosmological simulation, focusing on three star-forming disc galaxies with different SFHs. By assuming failed supernovae, we can predict an increasing trend of the gas-phase N/O–O/H abundance diagram, which was not produced in our previous simulations without failed supernovae. At high redshifts, contrary to the predictions of classical chemical evolution models with instantaneous mixing approximation, we find almost flat trends in the N/O–O/H diagram, which are due to the contribution of intermediate-mass stars together with an inhomogeneous chemical enrichment. Finally, we also predict that the average N/O and C/O steadily increase as functions of time, while the average C/N decreases, due to the mass and metallicity dependence of the yields of asymptotic giant branch stars; such variations are more marked during more intense star formation episodes. Our predictions on the CNO abundance evolution can be used to study the SFH of disc galaxies with the *James Webb* Space Telescope.

Key words. galaxies: abundances – galaxies: evolution – ISM: abundances – stars: abundances – hydrodynamics

1. Introduction

High-resolution multi-object spectrographs have made it possible to retrieve accurate information about the kinematics, chemical composition, ages and other fundamental physical properties for a very large ensemble of stars, putting strong constraints on the formation and evolution of our galaxy (e.g. Bensby et al. 2014; Hayden et al. 2015; Lindegren et al. 2016). Nevertheless, as soon as we enter into the broad field of extragalactic astronomy, our comprehension about how galaxies have formed and evolved with time becomes more uncertain, mostly because their global observed physical properties have usually been inferred from their integrated stellar light or emission lines.

Following the pioneering works by Garnett (1990) and Vila Costas & Edmunds (1993), emission line diagnostics are capable of measuring C, N, and O abundances, and are being applied to extragalactic systems, providing also the spatial distribution of the elemental abundances (e.g. Pilyugin et al. 2010; Sánchez-Menguiano et al. 2016; Belfiore et al. 2017; Toribio San Cipriano et al. 2017; Amorín et al. 2017). This blossoming of observational data will open a new window of interest for galactic astroarchaeology studies. In this respect, chemical evolution models – when included within cosmological hydrodynamical simulations and combined with spectrophotometric stellar population synthesis codes – can uniquely provide a powerful tool to unveil the past evolutionary history of galaxies. Only by dealing with the abundances of specific chemical elements (and hence only by shelving the generic observable "metallicity"), can we define sensitive chemical diagnostics of the entire star formation history (SFH) of the galaxy.

In this Letter, we present the results of our study on a sample of star-forming disc galaxies within an up-to-date cosmological hydrodynamical simulation, including a detailed routine for the galaxy chemical evolution (Kobayashi et al. 2007). We focus our analysis on the evolution of three examples of disc galaxies, representative of the different stellar systems within our catalogue, and show how their gas-phase chemical abundances of C, N, and O evolve as functions of the galaxy SFH. In Sect. 2, we briefly summarise the main characteristics and the setup of our simulation. In Sect. 3, we present the inhomogeneous enrichment and the global gas-phase CNO abundance evolution of our disc galaxies. Finally, in Sect. 4, we draw our conclusions.

## 2. Simulation model and assumptions

All the results of this Letter are obtained by running and analysing the outcome of a cosmological hydrodynamical simulation based on the GADGET-3 code (Springel 2005), which uses the smoothed particle hydrodynamics (SPH) method. Our code was developed by Kobayashi et al. (2007) to include the relevant physical processes related to the star formation activity and chemical evolution of galaxies (see also Taylor & Kobayashi 2014 for the details).

Chemical enrichment. The chemical evolution routine is the same as the one originally developed by Kobayashi (2004) for another SPH code, and gives an excellent agreement with the elemental abundance distributions as observed in the Milky Way (MW; Kobayashi & Nakasato 2011). In our model, we adopt the stellar yield set by Kobayashi et al. (2011) with failed Supernovae (SNe) at mass $m \geq 25 \, M_\odot$ and metallicity $Z \geq 0.02$, which are required from the observations of nearby SNe (e.g. Smartt 2009; see also the theoretical study of Müller et al. 2016). In failed SNe, all synthesised O and heavier elements fall back into the black hole, except for H, He, C, N, and F, which are synthesised in the outermost layers of the SN ejecta (Kobayashi et al., in prep.). Following Kobayashi et al. (2006), half of stars with $m \geq 25 \, M_\odot$ are assumed to explode as hypernovae. For the asymptotic giant branch (AGB) stars, we assume the same yields as in Kobayashi et al. (2011). Finally, we assume the Kroupa (2008) initial mass function (IMF), defined in the mass range $0.01 \leq m \leq 120 \, M_\odot$, and the same stellar lifetimes as in Kobayashi (2004).

Table 1. Main properties of our reference galaxies as functions of redshift.

| Galaxy name	Redshift	$M_\star$ [$M_\odot$]	f_{gas}	$\tau_{\star,1/2}$ [Gyr]	$\langle\tau_\star\rangle_V$ [Gyr]	$\langle Z_\star\rangle_V$	$r_{h,V}$ [kpc]	$\log(\langle N/O\rangle_V)$ dex	$\log(\langle C/O\rangle_V)$ dex	$\log(\langle C/N\rangle_V)$ dex
Galaxy A	$z = 0$	3.62×10^{10}	0.35	6.69	3.27	0.012	4.58	−0.85	−0.45	0.40
	$z = 0.5$	2.73×10^{10}	0.43	3.28	1.41	0.012	2.63	−0.84	−0.43	0.41
	$z = 1$	1.77×10^{10}	0.35	1.83	0.80	0.011	1.63	−0.91	−0.46	0.45
	$z = 2$	6.72×10^{9}	0.53	0.82	0.42	0.008	1.02	−1.00	−0.53	0.46
	$z = 3$	2.64×10^{9}	0.63	0.45	0.22	0.006	0.67	−1.12	−0.69	0.43
	$z = 4$	7.20×10^{8}	0.69	0.13	0.06	0.003	0.27	−1.39	−0.91	0.48
Galaxy B	$z = 0$	1.60×10^{10}	0.37	5.53	2.32	0.009	3.52	−0.87	−0.46	0.41
	$z = 0.5$	1.13×10^{10}	0.34	1.97	1.17	0.013	1.40	−0.87	−0.43	0.44
	$z = 1$	4.80×10^{9}	0.57	1.30	0.55	0.008	1.31	−1.05	−0.55	0.50
	$z = 2$	5.18×10^{8}	0.87	0.89	0.07	0.002	0.52	−1.43	−0.83	0.59
Galaxy C	$z = 0$	9.93×10^{9}	0.48	4.63	1.99	0.010	4.63	−0.90	−0.45	0.45
	$z = 0.5$	5.32×10^{9}	0.57	1.66	0.75	0.008	1.66	−1.05	−0.55	0.51
	$z = 1$	2.08×10^{9}	0.76	1.16	0.52	0.005	1.17	−1.16	−0.61	0.54

Notes. Columns are: (i) galaxy name; (ii) redshift; (iii) total galaxy stellar mass at the present time; (iv) fraction of gas within the galaxy with respect to the total baryonic mass (stellar plus gas content); (v) age at which half of the galaxy stellar mass originated; (vi) average V-band luminosity-weighted age; (vii) average stellar metallicity; (viii) galaxy disc half-light radius; (ix-x-xi) average stellar N/O, C/O and C/N ratios.
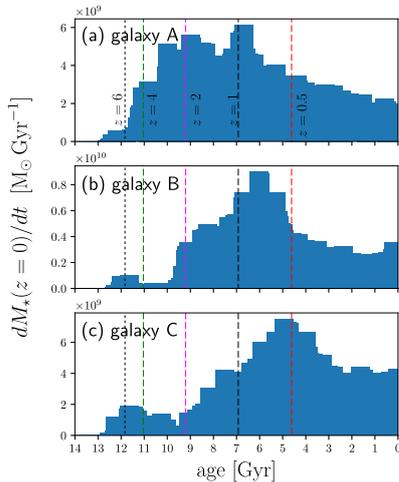
Fig. 1. Distribution of the present-day total stellar mass as a function of the star particle age. *Each panel* corresponds to one of our reference galaxies.

The photo-chemical code. In order to compute the average luminosity-weighted ages and metallicities of the galaxies in the simulation, as well as their half-light radii, we have developed a stellar population synthesis model[1], which is based on the one originally developed by Vincenzo et al. (2016b), assuming the PARSEC stellar evolutionary tracks (Bressan et al. 2012).

Simulation setup. Our assumed cosmological model is the standard Λ-cold dark matter Universe, with the same cosmological parameters as given by the nine-year Wilkinson Microwave Anisotropy Probe (Hinshaw et al. 2013). We follow the evolution of a cubic volume of the Universe, with periodic boundary conditions and side $\ell_U = 10\,\mathrm{Mpc\,h^{-1}}$, in comoving units. The initial conditions are the same as in Kobayashi et al. (2007), with improved resolution; $N_{DM} = N_{gas} = 128^3$ both for dark matter (DM) and gas particles. The feedback from the star formation activity and chemical evolution (i.e. the thermal energy and the nucleosynthetic products from stellar winds and SN explosions) is distributed to a number $N_{FB} = 576$ of neighbour gas particles, weighted by the
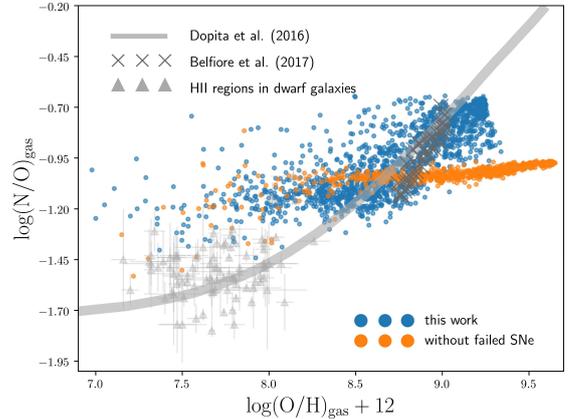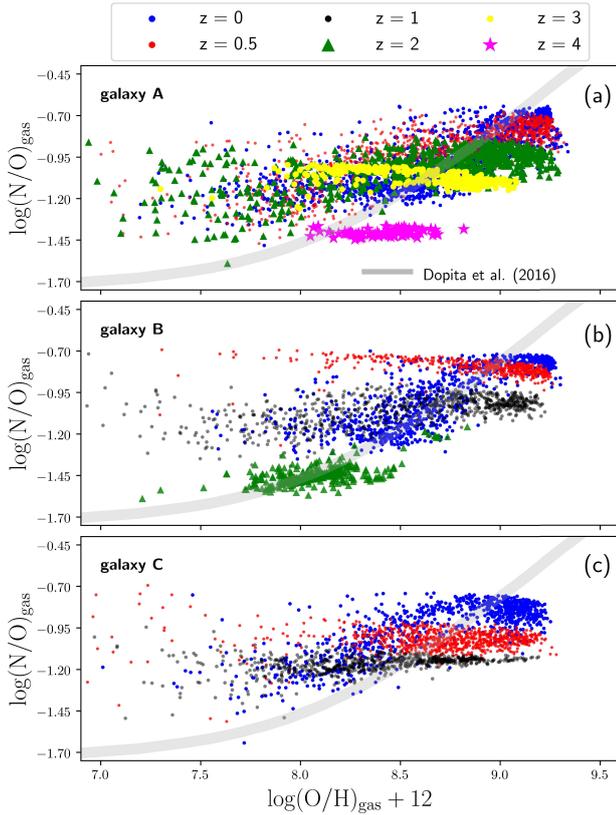

Fig. 2. Predicted gas-phase $\log(N/O)$ vs. $\log(O/H) + 12$ abundance pattern in Galaxy A with failed SNe (light blue points; this work) and without failed SNe (orange points). The solid grey line corresponds to the average relation obtained from various observations by Dopita et al. (2016, see references therein), the grey points with error bars to a compilation of data of individual HII regions in blue diffuse dwarf galaxies (Berg et al. 2012; Izotov et al. 2012; James et al. 2015), and the dark grey crosses to Belfiore et al. (2017) from a sample of spatially resolved galaxies from the MaNGa survey.

smoothing kernel. These parameters are determined to match the observed cosmic star formation rate (SFR; Hopkins & Beacom 2006; Madau & Dickinson 2014). Our simulation has the following mass resolutions: $M_{DM} \approx 3.097 \times 10^7\,\mathrm{h^{-1}}\,M_\odot$ and $M_{gas} = 6.09 \times 10^6\,\mathrm{h^{-1}}\,M_\odot$, for the DM and gas mass components, respectively. Finally, we assume a gravitational softening length $\epsilon_{gas} \approx 0.84\,\mathrm{h^{-1}}$ kpc, in comoving units.

3. Results

We analyse the outcome of our simulation, by creating a catalogue of stellar systems at redshift $z = 0$. We firstly make use of the friend-of-friends group-finding algorithm with adaptive hierarchical refinement ROCKSTAR (Behroozi et al. 2013) to create a catalogue of DM halos at redshift $z = 0$; from this catalogue, we isolate and analyse all the embedded stellar systems which are spatially clustered and contain a sufficient number of

---

[1] stri-cluster.herts.ac.uk/~fiorenzo

Fig. 3. Redshift evolution of the predicted gas-phase $\log(N/O)$ vs. $\log(O/H) + 12$ abundance patterns within our three reference galaxies. Galaxies A, B, and C clearly show different chemical evolution of the ISM abundances with redshift. We compare our simulation with the observed average N/O–O/H relation from Dopita et al. (2016, solid grey line).

both star and gas particles, so as to draw well sampled chemical abundance patterns. We exclude all the stellar systems which are undergoing a major merger at the present time. In total, we select ~ 35 galaxies with the aforementioned broad and simple criteria, lying within DM halos with virial mass in the range $11.0 \leq \log(M_{DM}/M_\odot) \leq 13.0$ dex (Vincenzo et al., in prep.).

In this Letter, we present the results of our analysis for three examples of star-forming disc galaxies, which have total stellar masses roughly of the same order of magnitude but are representative of distinct characteristic SFHs that are seen in the other disc galaxies in the simulation. In Table 1, we summarise the redshift evolution of the main predicted characteristics of our reference galaxies. The predicted stellar age distribution function of our galaxies is shown in Fig. 1. When passing from Galaxy C to Galaxy A, the emitted light at the present time is dominated by older stellar populations; the chemical enrichment also differs from galaxy to galaxy and all our reference galaxies end up at the present time by having almost the same average metallicity ($\langle Z_\star \rangle \sim 0.01$), following the observed mass-metallicity relation.

In Fig. 2, we show our predictions at redshift $z = 0$ for the gas-phase $\log(N/O)$ versus $\log(O/H) + 12$ abundance pattern in Galaxy A. Our results with failed SNe (light blue points) are compared with the same simulation but with the original Kobayashi et al. (2011)'s yields without failed SNe (orange points); each simulation point in the figure corresponds to one location within the galaxy. To understand the abundance patterns, we briefly recall that nitrogen is mostly synthesised by intermediate-mass stars by hot-bottom burning during the AGB phase. Most of the nitrogen from AGB stars is secondary and

its stellar yields steadily increase as functions of the initial stellar metallicity. All mass ranges of stars can also produce primary N, converted from ^{12}C by the CNO cycles (see also Vincenzo et al. 2016a and the references therein). Finally, oxygen is mostly produced by core-collapse SNe with very short lifetimes ($\sim 10^6$ yr).

In Fig. 2, with failed SNe, we find an increasing trend (of "secondary" production) at the metal-rich side of the N/O versus O/H diagram, predicting a similar slope as in observations. At very high metallicity, the increase may be slightly smaller than in the observed relation, which may be because stellar yields from super-solar AGB stars are not available (Vincenzo et al. 2016a). We also note that N and O might also be affected by dust depletion, which is not taken into account in our work. If we do not assume failed SNe, we have a much flatter slope at high metallicity, which is inconsistent with observations.

In Fig. 3, we show how the N/O–O/H relation evolves with redshift in our reference galaxies. There is a large scatter particularly at low O/H, which is due to inhomogeneous enrichment; in fact, there are gas particles that have gathered the nucleosynthetic products of only a few core-collapse SNe or AGB stars in the past (see Kobayashi & Nakasato 2011 for more details). When the galaxy is still experiencing its earliest evolutionary stages ($M_\star \sim 10^8 \, M_\odot$), the gas-phase N/O ratios are almost constant with metallicity, suggesting the presence of a plateau of "primary" production ($z \sim 4$ for Galaxy A; $z \sim 2$ for Galaxy B). This is not produced in classical one-zone chemical evolution models with instantaneous mixing approximation, which systematically underestimated N/O at very low metallicity and had to assume an artificial primary N production by massive stars (e.g. Matteucci 1986; Chiappini et al. 2005; Vincenzo et al. 2016a) to reproduce the observations at low metallicity in dwarf galaxies (Pilyugin et al. 2010; Berg et al. 2012; Izotov et al. 2012; James et al. 2015), damped-Lyα (DLA) absorption systems (e.g., Pettini et al. 2002, 2008), and MW halo stars (e.g., Spite et al. 2005).

We note that our predicted N/O plateau resides at larger O/H than in the HII regions of nearby dwarf galaxies, meaning that our reference galaxies were already more metal-rich at high redshifts than nearby dwarf galaxies. In the adopted yields, N/O from core-collapse SNe is much lower than in our high-redshift galaxies (~ -1.45 dex), but in the simulation there is already a significant contribution from AGB stars, which is the difference from the one-zone models. At lower redshifts ($M_\star \gtrsim 10^9 \, M_\odot$), the plateau exists but the value quickly reaches $\log(N/O) \sim -1.2$ dex with a larger contribution from AGB stars. Galaxy C is already at this phase when it is formed by a major merger at $z \sim 2$. We note that the plateau value would be even higher with the effects of stellar rotation.

In Fig. 4, we show how the average SFR-weighted gas-phase CNO abundances vary as functions of redshift for our reference galaxies; this diagram can be used for constraining the galaxy SFH. We only show the predictions of our simulation for the evolutionary times when the galaxy total stellar mass $M_\star(z) \geq 10^8 \, M_\odot$. In Fig. 4a the increase of the average N/O ratios turns out to be larger, corresponding to a more intense star formation episode (high-z in Galaxy A; low-z in Galaxy C). This is the typical imprint of strong chemical enrichment of secondary N from AGB stars.

In Fig. 4b and c, we show how the average SFR-weighted gas-phase $\log(C/O)$ and $\log(C/N)$ evolve with redshift. Carbon is mostly synthesised by low-mass stars with masses in the range $1 \lesssim m \lesssim 3 \, M_\odot$ (e.g. see Kobayashi et al. 2011). As for nitrogen, carbon can also be produced by core-collapse SNe, on short
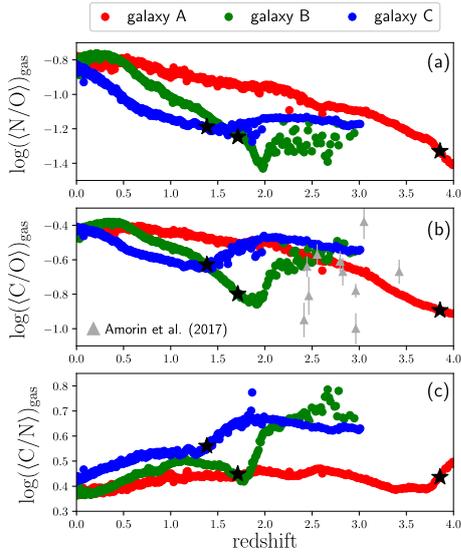
Fig. 4. *Panels a–c*: average SFR-weighted gas-phase $\log(N/O)$, $\log(C/O)$ and $\log(C/N)$ as functions of redshift. We only show the predictions of our simulation for the redshifts when the galaxy stellar mass $M_\star(z) \geq 10^8\ M_\odot$. The black star symbol on each track marks the redshift when $M_\star \approx 10^9\ M_\odot$. The grey triangles with the error bars correspond to the observational data of Amorín et al. (2017).

time-scales after the star formation event. With the IMF weighting, half of the C producers in galaxies are low-mass stars. The metallicity dependence of the C yields is opposite with respect to the metallicity dependence of the secondary N; while the produced secondary N steadily increases as a function of metallicity, the C yield steadily decreases.

In Fig. 4c, at high redshift, in the earliest galaxy evolutionary stages, we mostly witness at the chemical enrichment from massive stars with high C/N. The average C/N is subsequently predicted to sharply decrease at the onset of massive AGB stars. Then, C/N temporarily increases due to the C production of low-mass AGB stars; finally, C/N decreases again because of the opposite metallicy-dependence of the C and N stellar yields. Currently, observations at high redshifts are available for C/O ratios (Amorín et al. 2017), which roughly overlap with our model curves. The very low C/O ratios in Amorín et al. (2017) are consistent with the rapid and intense star formation in Galaxy A, but at much lower redshifts.

4. Conclusions

In this Letter, we have shown how the gas-phase C, N, and O abundances evolve as functions of the galaxy SFH. All our results have been obtained by analysing three examples of star-forming disc galaxies within a full cosmological hydrodynamical simulation, including up-to-date nucleosynthetic yields and a standard (non-variable) IMF.

Our simulation predicts an almost flat trend of N/O versus O/H at high redshifts, which is caused by an inhomogeneous enrichment of the galaxy ISM with a significant contribution of AGB stars at low metallicity. Our simulation represents an improvement with respect to previous chemical evolution models, both because the N/O–O/H relation was studied with simple one-zone models with instantaneous mixing approximation and because we did not assume any artificial primary N production by massive stars (Matteucci 1986; Chiappini et al. 2005; Vincenzo et al. 2016a). We note that the N/O plateau would be even higher if rapidly rotating massive stars were included.

We conclude that failed SNe are a very promising scenario to explain the observed trend of N/O vs. O/H. The inclusion of super-solar AGB stars might represent a further improvement of our model, since they can produce even larger amounts of secondary N as the metallicity increases, helping to explain the further increase of N/O at very high O/H.

The evolution of the gas-phase CNO abundances is driven by the chemical enrichment from AGB stars and core-collapse SNe, which create an increasing trend of the N/O and C/O towards higher metallicities by present. The predicted increase of the average N/O and C/O with redshift turns out to be faster within galaxies experiencing a more intense star formation activity during the considered redshift interval. Finally, in the earliest stages of galaxy evolution, we predict the largest C/N ratios and the lowest N/O ratios.

It is not easy to obtain both C and N for the same sample of galaxies with current observations, since the N/O and C/O ratios can only be estimated for $z \lesssim 2.5$ (optical rest frame) and $z \gtrsim 2 - 3$ (UV rest frame), respectively; in the near future, however, it will be possible to have measurements of C/N within galaxies at $z \lesssim 6$ with the Near-Infrared Spectrograph on the *James Webb* Space Telescope.

References

Amorín, R., Fontana, A., Pérez-Montero, E., et al. 2017, Nat. Astron., 1, 0052
Behroozi, P. S., Wechsler, R. H., & Wu, H.-Y. 2013, ApJ, 762, 109
Belfiore, F., Maiolino, R., Tremonti, C., et al. 2017, MNRAS, 469, 151
Bensby, T., Feltzing, S., & Oey, M. S. 2014, A&A, 562, A71
Berg, D. A., Skillman, E. D., Marble, A. R., et al. 2012, ApJ, 754, 98
Bressan, A., Marigo, P., Girardi, L., et al. 2012, MNRAS, 427, 127
Chiappini, C., Matteucci, F., & Ballero, S. K. 2005, A&A, 437, 429
Chiappini, C., Ekström, S., Meynet, G., et al. 2008, A&A, 479, L9
Dopita, M. A., Kewley, L. J., Sutherland, R. S., & Nicholls, D. C. 2016, Ap&SS, 361, 61
Garnett, D. R. 1990, ApJ, 363, 142
Hayden, M. R., Bovy, J., Holtzman, J. A., et al. 2015, ApJ, 808, 132
Hinshaw, G., Larson, D., Komatsu, E., et al. 2013, ApJS, 208, 19
Hopkins, A. M., & Beacom, J. F. 2006, ApJ, 651, 142
Izotov, Y. I., Thuan, T. X., & Guseva, N. G. 2012, A&A, 546, A122
James, B. L., Koposov, S., Stark, D. P., et al. 2015, MNRAS, 448, 2687
Kobayashi, C. 2004, MNRAS, 347, 740
Kobayashi, C., & Nakasato, N. 2011, ApJ, 729, 16
Kobayashi, C., Umeda, H., Nomoto, K., Tominaga, N., & Ohkubo, T. 2006, ApJ, 653, 1145
Kobayashi, C., Springel, V., & White, S. D. M. 2007, MNRAS, 376, 1465
Kobayashi, C., Karakas, A. I., & Umeda, H. 2011, MNRAS, 414, 3231
Kroupa, P. 2008, Pathways Through an Eclectic Universe, 390, 3
Lindegren, L., Lammers, U., Bastian, U., et al. 2016, A&A, 595, A4
Madau, P., & Dickinson, M. 2014, ARA&A, 52, 415
Matteucci, F. 1986, MNRAS, 221, 911
Müller, B., Heger, A., Liptai, D., & Cameron, J. B. 2016, MNRAS, 460, 742
Pettini, M., Ellison, S. L., Bergeron, J., & Petitjean, P. 2002, A&A, 391, 21
Pettini, M., Zych, B. J., Steidel, C. C., & Chaffee, F. H. 2008, MNRAS, 385, 2011
Pilyugin, L. S., Vílchez, J. M., & Thuan, T. X. 2010, ApJ, 720, 1738
Sánchez-Menguiano, L., Sánchez, S. F., Pérez, I., et al. 2016, A&A, 587, A70
Smartt, S. J. 2009, ARA&A, 47, 63
Spite, M., Cayrel, R., Plez, B., et al. 2005, A&A, 430, 655
Springel, V. 2005, MNRAS, 364, 1105
Taylor, P., & Kobayashi, C. 2014, MNRAS, 442, 2751
Toribio San Cipriano, L., Domínguez-Guzmán, G., Esteban, C., et al. 2017, MNRAS, 467, 3759
Vila Costas, M. B., & Edmunds, M. G. 1993, MNRAS, 265, 199
Vincenzo, F., Belfiore, F., Maiolino, R., Matteucci, & F., Ventura, P. 2016a, MNRAS, 458, 3466
Vincenzo, F., Matteucci, F., de Boer, T. J. L., Cignoni, M., & Tosi, M. 2016b, MNRAS, 460, 2238
Zafar, T., Centurión, M., Péroux, C., et al. 2014, MNRAS, 444, 744